Available online at www.sciencedirect.com

ScienceDirect

Ceramics International 41 (2015) 663–669

CERAMICS INTERNATIONAL

www.elsevier.com/locate/ceramint

Influence of Cr doping on structure and dielectric properties of $Li_xCr_yNi_{1-x-y}O$ ceramics

Jinda Khemprasit*, Bualan Khumpaitool

Materials Chemistry Research Center, Department of Chemistry and the Center of Excellence for Innovation in Chemistry, Faculty of Science, Khon Kaen University, Khon Kaen 40002, Thailand

Received 2 July 2014; received in revised form 22 August 2014; accepted 27 August 2014
Available online 4 September 2014

Abstract

$Li_xCr_yNi_{1-x-y}O$ (where $x=0.30$; $y=0.02$, 0.05, 0.10) ceramics were prepared using a sol–gel process and sintered at 1300 °C for 5 h. The sintered pellet samples were characterized using X-ray diffraction, scanning electron microscopy and transmission electron microscopy techniques. Dielectric properties were also investigated. All sintered samples exhibited only cubic rock-salt NiO structure and giant dielectric constants of $\sim 10^4$–10^5 over the measured frequency range with low loss tangents. Both values of dielectric constants and loss tangents decreased with increasing Cr content. This was related to the reduction of grain size as Cr content in LiCrNiO increased. Giant dielectric constants in these samples possibly resulted from boundary layer capacitor structures and partially from defect dipoles. The sample with Cr a molar ratio of 0.10 had the best dielectric properties with very high ε_r (4.76×10^4) and the lowest tanδ (0.46) measured at 10 kHz and room temperature.

Keywords: A. Sol–gel process; B. Grain size; C. Dielectric properties; LiCrNiO

1. Introduction

Lead-free dielectric materials with high dielectric constants are very attractive due to their potential impact in microelectronic device applications such as capacitors and memory devices. Recently, $CaCu_3Ti_4O_{12}$ (CCTO) [1–5] and (A, B)-codoped NiO systems with the formula $A_xB_yNi_{1-x-y}O$ [6–24] have been actively investigated due to their extraordinarily high dielectric constants ($\varepsilon_r \sim 10^4$-10^5) with weak temperature and frequency dependence. It has been widely thought that the boundary layer capacitors (BLCs) model is the most likely explanation of their dielectric behavior. In this model, the giant dielectric constant results from a heterogeneous microstructure consisting of semiconducting grains and insulating grain boundaries. Therefore, when an electric field is applied, the free charge carriers in semiconducting grains would accumulate at two edges of insulating grain boundary thin-layers, producing strong interfacial polarization. This is responsible for the high dielectric constant of such material systems, which can be tuned by changing the elements, A and B, in $A_xB_yNi_{1-x-y}O$ materials. Numerous authors reported tuned compositions of A (i.e., Li [6–13], Na [14], K [19]) and B (i.e., Al [7,17], Si [22], Ti [6,9,10,15,18], W [13], V [13,20], Cr [8,21], Co [11], Zr [12], Fe [16], Pr [23], Ta [24]). NiO is a Mott–Hubbard insulator at room temperature. However, doping with monovalent cations (A) can cause a considerable increase in the electrical conduction of NiO. It then becomes semiconductor due to point defects [25]. Meanwhile, addition of a transition metal (B) into NiO primarily accumulates at grain boundaries. Thus, the interior of grains is semiconductive (mainly Li-doped NiO) while the grain shells serve as insulating boundaries, as predicted by the BLCs model. As a simple series-layer model, the effective relative dielectric constant (ε_{re}) of BLCs structure can be simply expressed as [6,26]

$$\varepsilon_{re} = \varepsilon_r t_g / t_b$$

where t_g is the grain thickness, t_b is the grain boundary thickness, ε_r is the relative dielectric constant of the individual

*Corresponding author. Tel.: +66 43 202222x12371; fax: +66 43 202373.
E-mail address: jinda@kku.ac.th (J. Khemprasit).

http://dx.doi.org/10.1016/j.ceramint.2014.08.119
0272-8842/

element. It is notable that the effective relative dielectric constant depends upon t_g/t_b, relating to the microstructure and can be enhanced by a larger grain size. Wu and co-workers studied the dielectric behavior of $Li_xTi_yNi_{1-x-y}O$ (LTNO) with various concentrations where $x \leq 0.3$ and $y \leq 0.1$ [6]. They found that the Ti content had a remarkable effect upon the microstructure and dielectric constant of LTNO. With increasing Ti concentration, grain size reduction was observed, relating to a smaller t_g/t_b. This is predicted by the BLCs model. A decrease in the dielectric constant with increasing Ti content was seen. Manna's group reported the effect of Li doping upon the microstructure and dielectric properties of the $Li_xZr_yNi_{1-x-y}O$ ceramics [12]. The results showed that the dielectric constant increased with enhanced Li content due to an increase of grain size. Moreover, an addition of Li increased the grain conductivity, leading to an increase in the concentration of mobile charges inside the grain. As the result, more charges accumulated at the grain boundary, resulting in its huge dielectric constant. To obtain a huge dielectric constant and a low loss tangent, Cr was used as a dopant in LiNiO lattice with the stoichiometry of $Li_{0.30}Cr_{0.02}Ni_{0.68}O$ as reported by our group [8,21]. Huge dielectric constants ($\varepsilon_r \sim 10^4$–10^5) were observed in these materials. They could be partially enhanced through the BLCs mechanisms, which assumes that grain boundaries are less conducting (Cr-rich phase), while the grains are semiconducting. Thus, charges would accumulate at two edges of the insulator layers to form a micro-parallel capacitor, resulting in a huge dielectric constant. However, their loss tangents were still high. Therefore, to reduce the loss tangent, varying Cr concentration in $Li_xCr_yNi_{1-x-y}O$ (x=0.30; y=0.02, 0.05, 0.10) was investigated in the current research. These materials were prepared using a sol–gel process employing metal nitrates as starting materials and ethylene glycol as chelating agent. Moreover, the influence of Cr doping on structure and dielectric properties was studied. Electrical properties of grains and grain boundaries of these materials were investigated using impedance analysis.

2. Materials and methods

$Li_xCr_yNi_{1-x-y}O$ (where x=0.30; y=0.02, 0.05, 0.10) ceramics were prepared using a sol–gel process as follows. Stoichiometric amounts of starting materials, $LiNO_3$ (99%, ACROS), $Ni(NO_3)_2 \cdot 6H_2O$ (>97%, QRëC), were dissolved in deionized water and mixed with ethylene glycol as chelating agent to obtain clear green solutions. Aqueous $Cr(NO_3)_3 \cdot 9H_2O$ (99%, ACROS) in stoichiometric proportion was then gradually added to the solutions and refluxed for 2 h, followed by heating at 200 °C to obtain dried gels. The dried gels were calcined at 1000 °C for 3 h in air with a heating rate of 5 °C/min to get oxide powders. Then the oxide powders were ground and mixed with 3% polyvinyl acetate and then pressed into pellets with 11 mm diameter and 2–3 mm thickness using a hydraulic press. Finally, the pelletized samples were sintered at 1300 °C for 5 h. The sintered samples with various Cr concentrations are referred to as LCNO-C02, LCNO-C05 and LCNO-C10 for $Li_{0.30}Cr_{0.02}Ni_{0.68}O$, $Li_{0.30}Cr_{0.05}Ni_{0.65}O$ and $Li_{0.30}Cr_{0.10}Ni_{0.60}O$, respectively. Phase composition of the sintered pellet samples was identified using an X-ray diffractometer (XRD, D8 Advance) with monochromatic Cu $K\alpha$, a scan step of 0.02 from 20° to 80° (2θ). Microstructure of the sintered pellet samples was observed using scanning electron microscopy (SEM, LEO-1450VP) and transmission electron microscopy (TEM, Tecnai G^2 20, FEI) with an accelerating voltage of 200 kV. Capacitance and tanδ measurements were performed using an impedance analyzer (HP4194A, Agilent) at frequency range from 100 Hz to 1 MHz and at temperatures ranging from −40 °C to 150 °C.

3. Results and discussion

XRD patterns of the sintered LCNO pellet samples with various Cr concentrations are shown in Fig. 1. All patterns were nearly identical and showed main peaks at 37.4°, 43.6°, 63.3° and 75.8° which corresponded to the (1 1 1), (2 0 0), (2 2 0) and (3 1 1) planes, respectively, of the cubic rock-salt NiO structure [JCPDS No. 47-1049] without any secondary phases. This is consistent with previous research [21]. The crystallite size (D) was calculated using the Scherrer equation as follows:

$$D = (K\lambda)/(\beta \cos \theta)$$

where λ is the wavelength of the X-ray radiation, K is a constant as 0.9, β is the full-width at half-maximum height (FWHM) and θ is the diffraction angle. The crystallite sizes of the LCNO-C02, LCNO-C05 and LCNO-C10 sintered samples were 46.3, 47.9 and 46.0 nm, respectively (Table 1). The lattice parameters a of LCNO-C02, LCNO-C05 and LCNO-C10 were 4.129 Å, 4.155 Å and 4.147 Å, respectively (Table 1). They were slightly different and smaller than that of the standard value of 4.177 Å [JCPDS No. 47-1049]. This result was possibly explained by the substitution of smaller ions Li^+ (0.60 Å) and Cr^{3+} (0.61 Å) for larger Ni^{2+} ion (0.69 Å). When Cr^{3+} content increased, the lattice parameter should have decreased, but this result was not observed. This means that Cr^{3+} might have formed a secondary phase at the grain boundaries instead of substitution into the NiO lattice. However, that phase was not observed using XRD

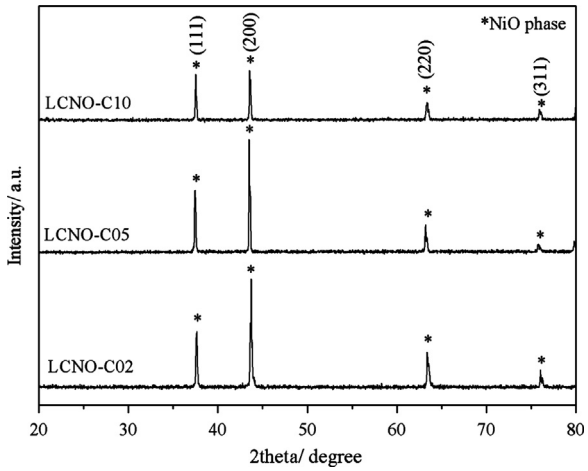

Fig. 1. XRD patterns of sintered LCNO pellet samples with various Cr concentrations.

Table 1
Summary of lattice parameters, crystallite sizes, relative density, grain size and dielectric properties of the sintered LCNO samples doped with different Cr contents at 10 kHz.

Sample	Lattice parameter a (Å)	Crystallite size (nm)	Relative density (%)	Grain size (μm)	ε_r at 10 kHz	tanδ at 10 kHz
LCNO-C02	4.129	46.3	95.26	60–120	2.24×10^5	1.48
LCNO-C05	4.155	47.9	93.39	20–90	4.33×10^4	0.64
LCNO-C10	4.147	46.0	81.38	10–35	4.76×10^4	0.46

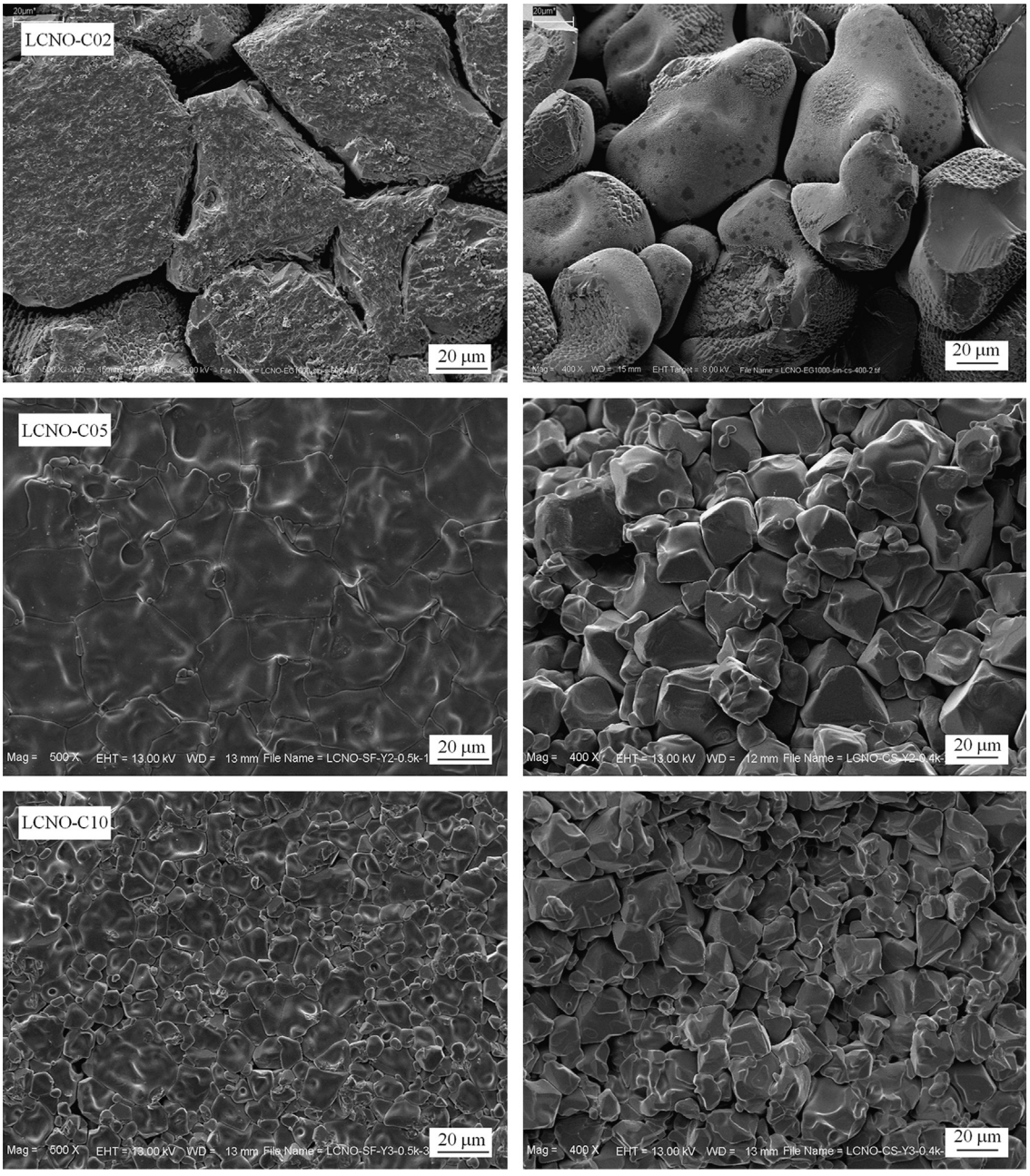

Fig. 2. SEM images of surfaces (left side) and fracture surfaces (right side) of sintered pellet samples with various Cr concentrations.

because of the method's limited sensitivity for small amounts of that phase.

Microstructures of the sintered LCNO pellet samples with different Cr contents are given in Fig. 2 (surfaces are shown in images on the left; fractured surfaces are seen in the right side images). Polyhedral grains with agglomerations were observed in all samples. The grain sizes of LCNO-C02, LCNO-C05 and LCNO-C10 were 60–120, 20–90 and 10–35 μm, respectively,

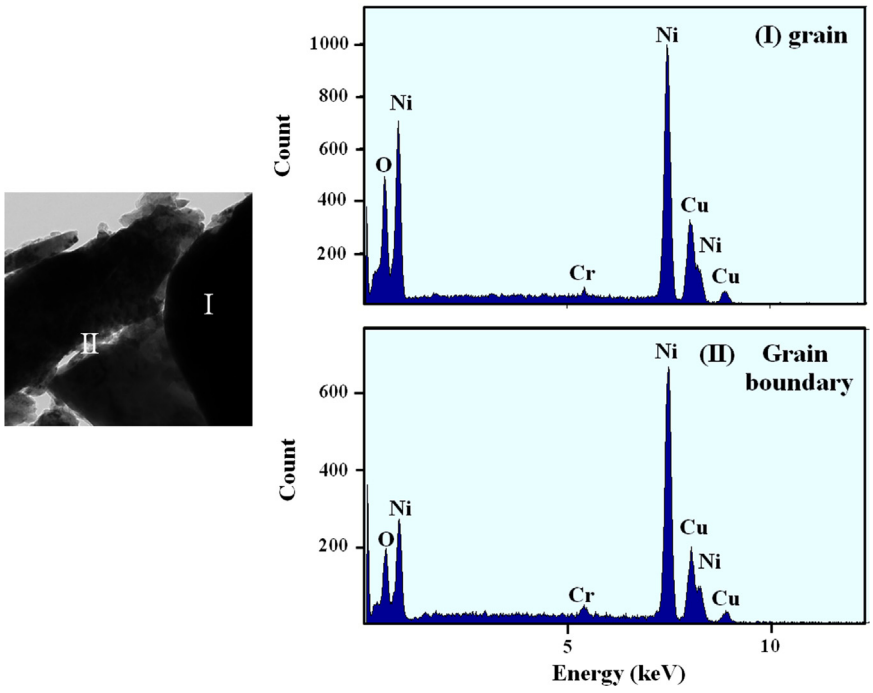

Fig. 3. TEM image of the sintered LCNO-C02 sample and EDX spectra of different regions.

as given in Table 1. It was also found that the grain size decreased with increasing Cr concentration. The reduction of grain size was consistent with the results in other studies [7,8]. This was possibly due to the existence of secondary phases at the grain boundaries, leading to a suppression of grain growth. However, the grain size is normally larger than the crystallite size calculated from XRD result because of agglomeration of very small particles. The element composition of LCNO at the grain and grain boundary regions can be investigated by energy-dispersive X-ray spectroscopy (EDX) as shown in Fig. 3. The atomic ratio of Cr/Ni at the grain boundaries was 0.048, which was higher than at the grain region (Cr/Ni=0.018). This implied that a Cr-rich phase at grain boundaries probably inhibited the grain growth. The presence of Cr in both grains and grain boundaries can occur if the Cr component has entered grains and grain boundaries [7,9]. The peak of Cu resulted from Cu grid supporting the sample. No trace of a Li phase was detected in EDX spectra because its atomic number was too low for this method. The relative densities of all sintered pellet samples with various Cr concentrations are given in Table 1. It can be seen that the relative densities decreased from 95.26% to 81.38% as Cr content increased. This was related to development of pores in samples with higher Cr content.

Frequency dependence of dielectric properties of the sintered LCNO pellet samples with various Cr contents is shown in Fig. 4. It was found that a gradual decline of ε_r occurred for LCNO-C02 while the weak frequency dependence of ε_r over a wide frequency range was observed in LCNO-C05 and LCNO-C10 samples as frequency increased. The large ε_r at low frequency is explained on the basis of space charge polarization. However, all samples exhibited very large ε_r ($\sim 10^4$–10^5) over the frequency range from 100 Hz to 1 MHz. This is in agreement with works dealing with NiO-based systems [6,8,10–12,21]. As frequency increased, tanδ rapidly decreased and then remained nearly

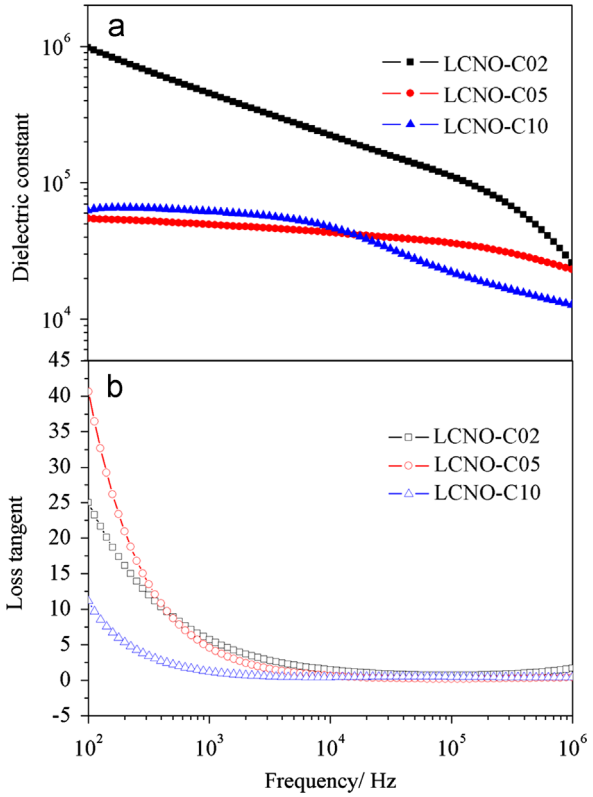

Fig. 4. Frequency dependence of (a) dielectric constant and (b) loss tangent of the sintered LCNO pellet samples with various Cr concentrations at room temperature.

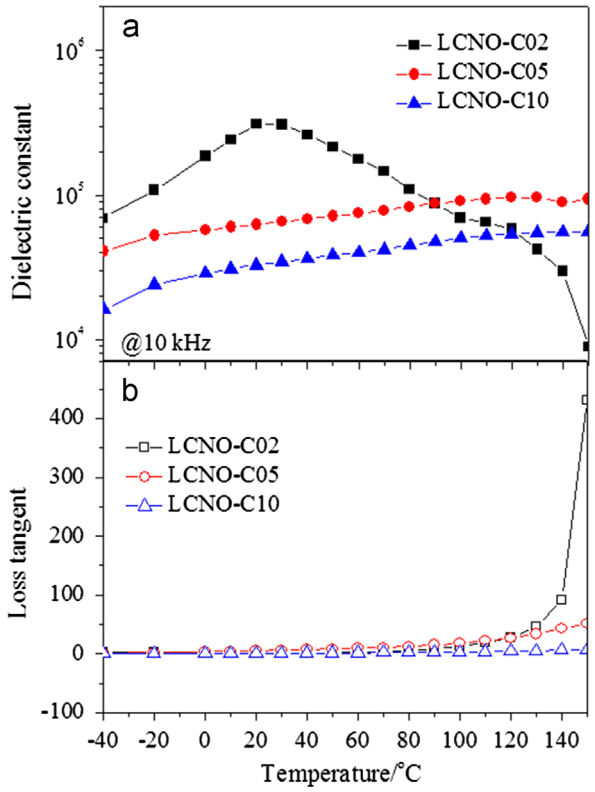

Fig. 5. Temperature dependence of (a) dielectric constant and (b) loss tangent measured at 10 kHz of the sintered LCNO pellet samples with various Cr concentrations.

constant in the frequency range of 10 kHz to 1 MHz for all samples.

Fig. 5 shows the temperature dependence of dielectric properties measured over the temperature range of −40 °C to 150 °C at 10 kHz. The results showed that both ε_r and tanδ of the sintered LCNO-C05 and LCNO-C10 pellet samples were weakly temperature dependent over a wide temperature range. A strong temperature dependence was observed in the LCNO-C02 sample with the peak of ε_r at ~25 °C. This is consistent with published literature [10]. Furthermore, tanδ of LCNO-C02 was very high at higher temperatures resulting from the dc conductivity contribution as earlier reported [6,10]. A summary of ε_r and tanδ values at room temperature at a frequency of 10 kHz for all sintered LCNO samples is given in Table 1. Appropriate dielectric properties with very high ε_r and the lowest tanδ were observed in LCNO-C10 ($\varepsilon_r = 4.76 \times 10^4$, tan$\delta$ = 0.46 at 10 kHz). Its ε_r was higher than that of CCTO ceramics [1,2], $Li_{0.01}M_{0.05}Ni_{0.94}O$ (M=W, V) [13] and (Na, Ti)-doped NiO [14], (Li, Al)-doped NiO [7,17], $Li_{0.05}Ti_{0.02}Ni_{0.93}O$ [18], $M_{0.03}Ti_{0.10}Ni_{0.87}O$ (M = K, Mg, Y) [19]. Its tanδ was lower than that of NiO-based ceramics [16,20,27]. It is notable that the tanδ obtained in this study was lower than reported in our previous work (tanδ =5.73) [21] as was expected.

The huge dielectric constants observed in these ceramics could be partially enhanced through the BLCs mechanism as seen in other studies [4,6,10]. Grain boundaries are less

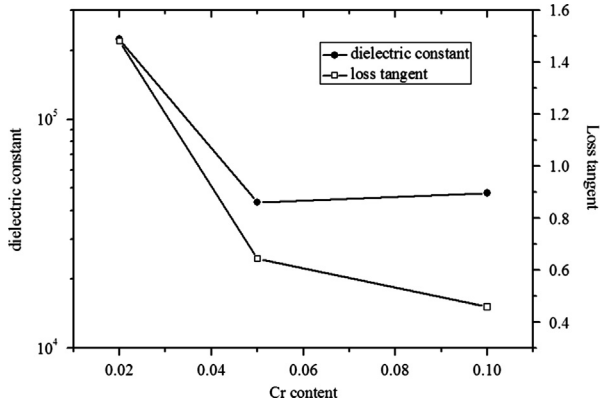

Fig. 6. Variation of ε_r and tanδ at 10 kHz and room temperature of the sintered LCNO pellet samples as a function of Cr content.

conductive (as indicated by the Cr-rich phase observed in EDX), while the grains are semiconductive. Therefore, when an electric field is applied, opposite charges accumulate at two edges of the insulator layers to form a micro-parallel capacitor. If the grain interior has more polarization via charge conduction, a large dielectric constant would result. Moreover, a giant dielectric constant may result from defect dipoles. With Cr^{3+} doping, Ni^{2+} sites could be occupied by Cr^{3+} ions. Defects can be introduced inside the grain of LCNO samples due to the different valences of Ni^{2+} and Cr^{3+} ions, as follows:

$$Cr_2O_3 \xrightarrow{NiO} 2Cr_{Ni}^{\bullet} + V_{Ni}^{''} + 3O_o^x$$

Consequently, the dielectric constant is partially influenced by the defect dipoles generated by $V_{Ni}^{''}$ vacancies as reported in earlier works [7,9,11]. Variation of ε_r and tanδ at 10 kHz and room temperature as a function of Cr content is shown in Fig. 6. It was found that ε_r and tanδ tended to decrease with increasing Cr content. According to the BLCs model, a decrease of ε_r can be attributed to a decrease in grain size. A decrease in grain size leads to decreased volume of polarization while increasing in the internal boundaries that block ions and charge carriers involving in the process of conduction within the sample. This behavior also reduces tanδ in NiO-based ceramics [7,10,17].

Impedance analysis is a tool to separate the electrical response in the grain and grain boundary to characterize the electrical properties of the sintered LCNO samples of varying Cr content. The impedance data of each sintered LCNO samples at different Cr contents and selected temperatures are shown in Fig. 7. The result showed that a large semicircular arc with a non-zero intercept on the Z' axis at high frequency (near origin) represented the contribution of grains, while the low frequency arc represented the contribution of grain boundaries (GB). The nonzero intercept on the Z' axis indicated that the presence of an arc was related to semiconducting grain and was beyond the maximum measured frequency (1 MHz). This result was similar to that observed in CCTO [3] and (Li, V)-doped NiO [20] ceramics. Although, the nonzero intercept on the real Z' axis was obtained, it was important to note that the resistance of the

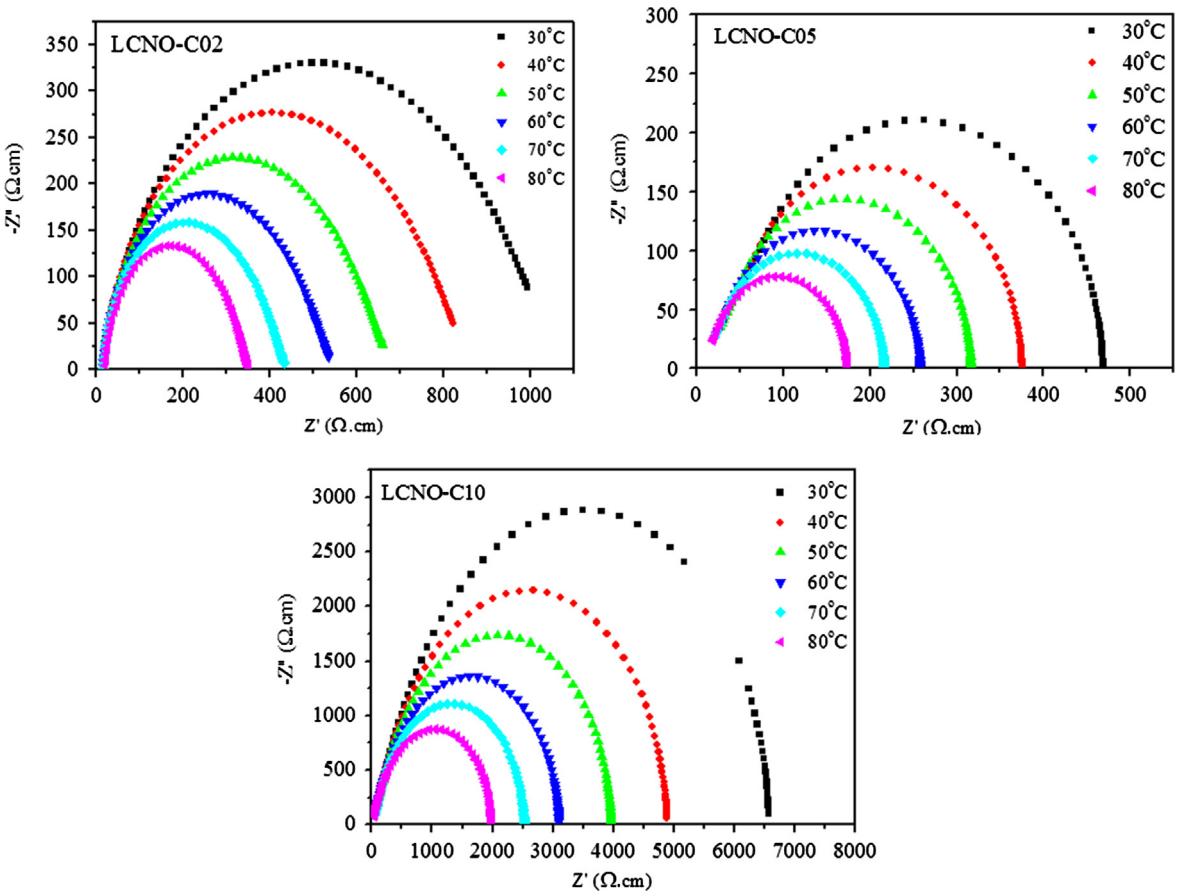

Fig. 7. Impedance spectra at selected temperatures for the sintered LCNO samples with various Cr contents.

grain boundary (R_{gb}) was larger than that of the grain (R_g) by 2–3 orders of the magnitude. As a result, it is reasonable to conclude that the LCNO ceramics had the different electrical responses, consisting of semiconducting grains and insulating GB. All impedance data can be modeled on an equivalent circuit based upon two parallel (resistor, R and capacitor, C) elements connected in series. One RC element corresponded to the semiconducting grains and the other RC element modeled insulating GB regions. In order to obtain R_g and R_{gb} by the proportional fitting on the Z' axis, the conductivity data (σ) can be estimated using the Arrhenius law,

$$\sigma \propto T^{-1}\exp\left(-E/k_BT\right)$$

where E is the activation energy for conduction, k_B is the Boltzmann constant and T is the absolute temperature. Fig. 8 shows the Arrhenius plots of grain and GB conductivity data for the sintered LCNO with various Cr contents. The conduction activation energy of grain (E_g) and GB (E_{gb}) were determined. The values of E_g were 0.110, 0.119 and 0.118 eV, E_{gb} were 0.210, 0.282 and 0.269 eV for LCNO-C02, LCNO-C05 and LCNO-C10, respectively. These values were consistent with those observed in (Li, Zr)-doped NiO [12]. It can be seen that the conduction activation energies of the grain interiors were smaller than those of the grain boundaries. This indicates an electrically heterogeneous microstructure with different mechanisms of electrical transport in the grains and grain boundaries. From these results, it is reasonable that high dielectric constants in LCNO ceramics were observed.

4. Conclusions

Li and Cr co-doped NiO ceramics with various Cr contents were successfully prepared using a sol–gel process. All sintered LCNO pellet samples had a single phase of cubic rock-salt NiO structure with nanoscale crystallite sizes and polyhedral grains with agglomeration. Moreover, grain sizes decreased with increasing Cr concentration. This was probably due to an existence of secondary phases at grain boundaries, leading to a suppression of the grain growth. All sintered samples also exhibited giant dielectric constants of about 10^4–10^5 over the measured frequency range, partially resulting from BLCs structure and partially from defect dipoles. Values of ε_r and tanδ decreased as Cr content increased, relating to reduction of grain sizes. The best dielectric properties were observed in $Li_{0.30}Cr_{0.10}Ni_{0.60}O$ where the ε_r was 4.76×10^4 and tanδ was 0.46 at 10 kHz and room temperature. The E_g and E_{gb} values of this sample were 0.118 and 0.269 eV, respectively, indicating different electrical transport mechanisms in the grain and grain boundary. Their microstructure was electrically heterogeneous. This behavior results in giant dielectric constants.

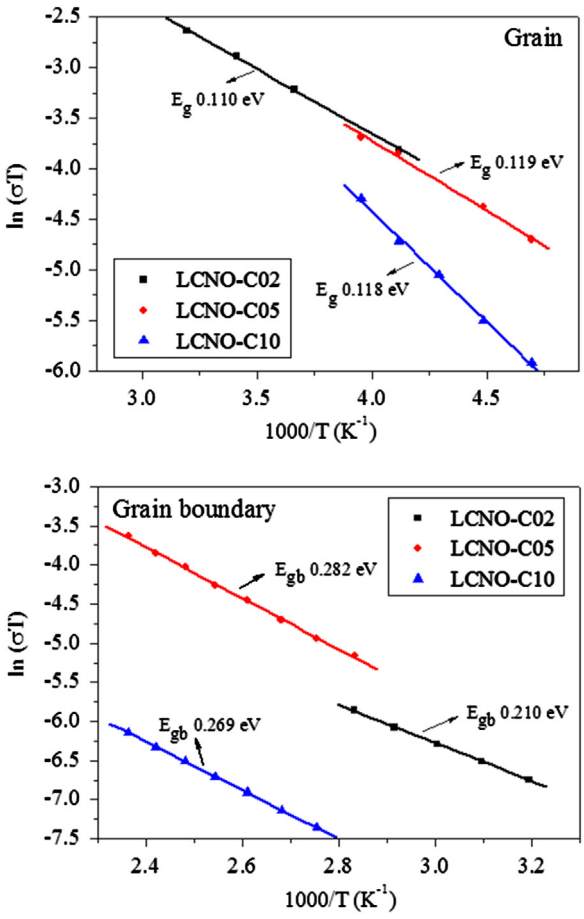

Fig. 8. Arrhenius plots of the grain and grain boundary conductivity data for the sintered LCNO samples with different Cr contents.

Acknowledgements

This work was financially supported by the Higher Education Research Promotion and National Research University Project of Thailand, Office of the Higher Education Commission, through the Advanced Functional Materials Cluster of Khon Kaen University, and by the Center of Excellence for Innovation in Chemistry (PERCH-CIC), Commission on Higher Education, Ministry of Education. The authors would like to thank the National Metal and Materials Technology Center (MTEC) for dielectric properties measurement, and the Department of Environmental Engineering, Faculty of Engineering, Khon Kaen University, for providing use of their XRD facility.

References

[1] M.A. Subramanian, D. Li, N. Duan, B.A. Reisner, A.W. Sleight, High dielectric constant in $ACu_3Ti_4O_{12}$ and $ACu_3Ti_3FeO_{12}$ phases, J. Solid State Chem. 151 (2000) 323–325.

[2] A.P. Ramirez, M.A. Subramanian, M. Gardel, G. Blumberg, D. Li, T. Vogt, S.M. Shapiro, Giant dielectric constant response in a copper-titanate, Solid State Commun. 115 (2000) 217–220.

[3] D.C. Sinclair, T.B. Adams, F.D. Morrison, A.R. West, $CaCu_3Ti_4O_{12}$: one-step internal barrier layer capacitor, Appl. Phys. Lett. 80 (2002) 2153–2155.

[4] R. Schmidt, M.C. Stennett, N.C. Hyatt, J. Pokorny, J.P. Gonjal, M. Li, D.C. Sinclair, Effects of sintering temperature on the internal barrier layer capacitor (IBLC) structure in $CaCu_3Ti_4O_{12}$ (CCTO) ceramics, J. Eur. Ceram. Soc. 32 (2012) 3313–3323.

[5] S. Jesurani, S. Kanagesan, M. Hashim, I. Ismail, Dielectric properties of Zr doped $CaCu_3Ti_4O_{12}$ synthesized by sol–gel route, J. Alloys Compd 551 (2013) 456–462.

[6] J. Wu, C.W. Nan, Y. Lin, Y. Deng, Giant dielectric permittivity observed in Li and Ti doped NiO, Phys. Rev. Lett. 89 (2002) 217601.

[7] S. Tangwancharoen, P. Thongbai, T. Yamwong, S. Maensiri, Dielectric and electrical properties of giant dielectric (Li, Al)-doped NiO ceramics, Mater. Chem. Phys. 115 (2009) 585–589.

[8] B. Khumpaitool, J. Khemprasit, Improvement in dielectric properties of Al_2O_3-doped $Li_{0.30}Cr_{0.02}Ni_{0.68}O$ ceramics, Mater. Lett. 65 (2011) 1053–1056.

[9] Y. Lin, R. Zhao, J. Wang, J. Cai, C.W. Nan, Y. Wang, L. Wei, Polarization of high-permittivity dielectric NiO-based ceramics, J. Am. Ceram. Soc. 88 (2005) 1808–1811.

[10] S. Maensiri, P. Thongbai, T. Yamwong, Giant dielectric response in (Li, Ti)-doped NiO ceramics synthesized by the polymerized complex method, Acta Mater. 55 (2007) 2851–2861.

[11] Y. Li, L. Fang, L. Liu, Y. Huang, C. Hu, Giant dielectric response and charge compensation of Li- and Co-doped NiO ceramics, Mater. Sci. Eng., B 177 (2012) 673–677.

[12] S. Manna, S.K. De, Giant dielectric permittivity observed in Li and Zr co-doped NiO, Solid State Commun. 150 (2010) 399–404.

[13] G.J. Chen, Y.J. Hsiao, Y.S. Chang, Y.L. Chai, Structure and high dielectric permittivity of $Li_{0.01}M_{0.05}Ni_{0.94}O$ (M=V and W) ceramics, J. Alloys Compd 474 (2009) 237–240.

[14] P.K. Jana, S. Sarkar, H. Sakata, T. Watanabe, B.K. Chaudhuri, Microstructure and dielectric properties of $Na_xTi_yNi_{1-x-y}O$ (x=0.05–0.30, y=0.02), J. Phys. D: Appl. Phys 41 (2008) 065403.

[15] Y.H. Lin, M. Li, C.W. Nan, J. Li, J. Wu, J. He, Grain and grain boundary effects in high-permittivity dielectric NiO-based ceramics, Appl. Phys. Lett. 89 (2006) 032907.

[16] P. Thongbai, S. Pongha, T. Yamwong, S. Maensiri, Effects of Fe, Ti, and V doping on the microstructure and electrical properties of grain and grain boundary of giant dielectric NiO-based ceramics, Appl. Phys. Lett. 94 (2009) 022908.

[17] Y. Lin, J. Wang, L. Jiang, Y. Chen, C.W. Nan, High permittivity Li and Al doped NiO ceramics, Appl. Phys. Lett. 85 (2004) 5664–5666.

[18] P. Thongbai, T. Yamwong, S. Maensiri, The sintering temperature effects on the electrical and dielectric properties of $Li_{0.05}Ti_{0.02}Ni_{0.93}O$ ceramics prepared by a direct thermal decomposition method, J. Appl. Phys. 104 (2008) 074109.

[19] B. Cheng, Y.H. Lin, A. Mei, J.N. Cai, C.W. Nan, J. He, Effects of grain modification on the dielectric properties of $A_{0.03}Ti_{0.10}Ni_{0.87}O$ (A: K^+, Mg^{2+}, Y^{3+}) ceramics, Appl. Phys. Lett. 92 (2008) 142903.

[20] S. Pongha, P. Thongbai, T. Yamwong, S. Maensiri, Giant dielectric response and polarization relaxation mechanism in (Li, V)-doped NiO ceramics, Scr. Mater. 60 (2009) 870–873.

[21] B. Khumpaitool, J. Khemprasit, Effect of calcining temperature on structural and dielectric properties of $Li_{0.30}Cr_{0.02}Ni_{0.68}O$ ceramics, J. Alloys Compd 587 (2014) 211–216.

[22] Y. Lin, L. Jiang, R. Zhao, C.W. Nan, High-permittivity core/shell structured NiO-based ceramics and their dielectric response mechanism, Phys. Rev. B: Condens. Matter 72 (2005) 014103.

[23] A.A. Dakhel, Giant dielectric permittivity in Li and Pr co-doped NiO ceramics, J. Alloys Compd 488 (2009) 31–34.

[24] Y.J. Hsiao, Y.S. Chang, T.H. Fang, Y.L. Chai, C.Y. Chung, Y.H. Chang, High dielectric permittivity of Li and Ta codoped NiO ceramics, J. Phys. D: Appl. Phys 40 (2007) 863–868.

[25] J.V. Elp, H. Eskes, P. Kuiper, G.A. Sawatzky, Electronic structure of Li-doped NiO, Phys. Rev. B: Condens. Matter 45 (1992) 1612–1622.

[26] A.J. Moulson, J.M. Herbert, Electroceramics, second ed., John Wiley & Sons, England, 2003.

[27] A.A. Dakhel, Dielectric relaxation behavior of Li and La co-doped NiO ceramics, Ceram. Int. 39 (2013) 4263–4268.